PCCP



PAPER View Article Online
View Journal | View Issue



Cite this: *Phys. Chem. Chem. Phys.*, 2021, **23**, 5113

Density matrix and purity evolution in dissipative two-level systems: I. Theory and path integral results for tunneling dynamics

Sambarta Chatterjee (Da and Nancy Makri (D *ab

The time evolution of the purity (the trace of the square of the reduced density matrix) and von Neumann entropy in a symmetric two-level system coupled to a dissipative harmonic bath is investigated through analytical arguments and accurate path integral calculations on simple models and the singly excited bacteriochlorophyll dimer. A simple theoretical analysis establishes bounds and limiting behaviors. The contributions to purity from a purely incoherent term obtained from the diagonal elements of the reduced density matrix, a term associated with the difference of the two eigenstate populations, and a third term related to the square of the time derivative of a site population, are discussed in various regimes. In the case of tunneling dynamics from a localized initial condition, the complex interplay among these contributions leads to the recovery of purity under low-temperature, weakly dissipative conditions. Memory effects from the bath are found to play a critical role to the dynamics of purity. It is shown that the strictly quantum mechanical decoherence process associated with spontaneous phonon emission is responsible for the long-time recovery of purity. These analytical and numerical results show clearly that the loss of quantum coherence during the evolution toward equilibrium does not necessarily imply the decay of purity, and that the time scales relevant to these two processes may be entirely different.

Received 22nd October 2020, Accepted 18th February 2021

DOI: 10.1039/d0cp05527a

rsc.li/pccp

I. Introduction

Quantum coherence continues to be a subject of intense theoretical and experimental interest, not only because of its intriguing manifestations, but also because of important technological prospects related to the design of nanoscale devices, solar energy harvest and quantum computers. In the context of dynamics, quantum coherence usually refers to the beating patterns that arise from the superposition of two or more quantum states which evolve with different phases. Unfortunately, the delicate nature of phase relations that enable quantum coherence¹ makes such phenomena extremely difficult to sustain, and the textbook-type oscillatory patterns characteristic of small isolated molecules tend to be destroyed by the dissipative effects of a system's environment.

For almost four decades, the model of a two-level system (TLS) coupled to a harmonic dissipative bath has served as the paradigm of quantum coherence and its destruction. With simple forms of the collective parameters defining the bath, the tunneling dynamics of this system undergoes a transition

from damped oscillations to monotonic decay and even complete localization.² A plethora of analytical and computational treatments have established the specifics of such dynamical effects. The complex interplay among coherent tunneling and thermal fluctuations leads to interesting phenomena in barrier crossing dynamics^{3–5} and nonadiabatic processes,^{6–9} which are ubiquitous in proton transfer reactions¹⁰ and charge transfer.^{11,12}

The decay of the purity or idempotence of a system's reduced density matrix (RDM) $\tilde{\rho}$ has often been used as a basis-independent measure of decoherence. The purity is defined as

$$Q(t) = \operatorname{Tr}\tilde{\rho}(t)^{2}.$$
 (1.1)

A common measure of disorder and information loss is a system's entropy. The most widely employed statistical mechanical definition of the latter is the von Neumann entropy, given by the expression

$$S(t) = -\operatorname{Tr}\tilde{\rho}(t)\ln\tilde{\rho}(t), \tag{1.2}$$

which (by design) is an extensive property. Another definition, with a simpler functional form, is the linear entropy, $S_{\rm lin} = 1 - {\rm Tr} \tilde{\rho}(t)^2$, which is directly related to the purity. It is often assumed that as a system, initially placed in a non-stationary

^a Department of Chemistry, University of Illinois, Urbana, IL 61801, USA. E-mail: nmakri@illlinois.edu

^b Department of Physics, University of Illinois, Urbana, IL 61801, USA

pure state, loses coherence through interactions with a dissipative environment, its purity also decays within a similar characteristic time. Estimates of purity decay time have been obtained using short-time perturbative treatments and some numerical calculations. ^{13–17}

In a recent Letter, 18 we showed that the time evolution of purity can be considerably more complex. In particular, we presented accurate numerical results which show that the purity of an initially localized TLS can recover substantially following an early drop. We found that the evolution of purity is governed by the interplay among three physically meaningful components, which can lead to non-monotonic timedependence, and that its recovery can be nearly complete at low temperature and under weakly dissipative conditions. These findings should not be surprising, as the long-time value of purity is related to the equilibrium RDM, which under favorable conditions is dominated by the TLS ground state. While a TLS eigenstate is a coherent superposition of the right- and leftlocalized states, an eigenstate does not display phase beating. Thus, once equilibrium is reached, dynamical observables remain stationary and dynamical coherence has ended. The recovery of purity when the TLS coherence has been completely lost, along with the fact that under some conditions the purity attains its minimum value early on, when the TLS still exhibits largeamplitude tunneling oscillations, suggest that purity should not be used as a measure of quantum coherence and its destruction by the environment. In particular, the short time associated with the early decrease of purity is not necessarily characteristic of the time associated with quantum coherence from phase beating. Earlier work¹⁹ using forward-backward semiclassical methods to examine the dynamics of an anharmonic oscillator coupled to a harmonic bath also identified minor oscillatory components (but not a recovery) in the evolution of purity and concluded that the time scales of decoherence and purity can differ substantially.

The present paper presents a comprehensive study of RDM evolution and its purity in the tunneling dynamics of a symmetric TLS coupled to a dissipative bath. We begin by presenting in section II a simple theoretical analysis that establishes key properties in the early-time and equilibrium value of purity, along with some considerations that concern its behavior, regardless of the system's initial preparation. Specifically, we establish various inequalities and limiting behaviors, and review the decomposition of purity in terms of three physically meaningful components identified in ref. 18. We also analyze the role of classical and quantum decoherence effects, which are associated with level fluctuations and spontaneous phonon emission processes, 20 on the evolution of purity. In section III we specialize on the time evolution of purity with a localized initial state and use very simple arguments to show that the early dynamics of purity is through leading order quadratic (or, equivalently, Gaussian), in agreement with the result of power series expansions²¹ and perturbative treatments. 13,15-17 However, we show in the companion article²⁴ (Paper II) that, under different initial conditions, the early evolution of purity can also be a growing function. This analysis and conclusions pertain to a symmetric TLS in contact with a generic dissipative environment, which is not restricted to a harmonic bath.

In Section IV we specialize to a TLS system interacting with a dissipative harmonic bath. We investigate the time evolution of purity under a variety of conditions and its dependence on system-bath coupling strength, temperature, and the frequency composition of the bath, using numerically exact, fully quantum mechanical real-time path integral calculations. We also analyze the origin of the observed patterns, along with the underlying mechanism of these processes. In section V we investigate the evolution of purity during the excitation energy transfer in the bacteriochlorophyll dimer at room temperature through calculations that include all intramolecular normal modes with nonzero Huang–Rhys factors. Our calculations indicate that a significant recovery of purity is possible in large molecular systems under physiological conditions. A summary of our results is given in Section VI, along with some concluding remarks.

II. General theoretical considerations

(i) Dissipative two-level system

The focus of this work is on a two-level quantum system bilinearly coupled to a bath of harmonic oscillators, which displays the complex interplay between the important, fundamentally quantum mechanical phenomenon of tunneling and the decohering effects of an environment. In the local (or site) basis, the symmetric TLS Hamiltonian has the form

$$\hat{H}_{\text{TLS}} = -\hbar\Omega(|\mathbf{R}\rangle\langle\mathbf{L}| + |\mathbf{L}\rangle\langle\mathbf{R}|) \tag{2.1}$$

where $|R\rangle$ and $|L\rangle$ are the right- and left-localized states. The eigenstates of eqn (2.1) are the sum and difference of the localized states,

$$|\Phi_0\rangle = \frac{1}{\sqrt{2}}(|R\rangle + |L\rangle), \quad |\Phi_1\rangle = \frac{1}{\sqrt{2}}(|R\rangle - |L\rangle)$$
 (2.2)

and the tunneling splitting is $2\hbar\Omega$. The TLS is coupled to a harmonic bath through the additional term

$$\hat{H}_{\text{bath}} = \sum_{j} \frac{\hat{p}_{j}^{2}}{2m_{j}} + \frac{1}{2}m_{j}\omega_{j}^{2}\hat{q}_{j}^{2} - c_{j}\hat{q}_{j}(|R\rangle\langle R| - |L\rangle\langle L|). \quad (2.3)$$

The effects of the bath on the dynamics of the TLS are collectively described by the spectral density function²²

$$J(\omega) = \frac{1}{2}\pi \sum_{j} \frac{c_{j}^{2}}{m_{j}\omega_{j}} \delta(\omega - \omega_{j}). \tag{2.4}$$

In this work we employ the common Ohmic spectral density with an exponential cutoff,²

$$J(\omega) = \frac{1}{2}\pi\hbar\xi\omega e^{-\omega/\omega_{\rm c}}, \qquad (2.5)$$

where the dimensionless Kondo parameter ξ quantifies the system-bath coupling strength and ω_c is the bath cutoff frequency, which corresponds to the maximum of the spectral density. The overall strength of system-bath coupling is often characterized in terms of the bath reorganization energy, ¹¹

$$\lambda = \frac{4}{\pi} \int_0^\infty \frac{J(\omega)}{\omega} d\omega. \tag{2.6}$$

For a bath described by an Ohmic spectral density, the reorganization energy is $\lambda = 2\hbar \xi \omega_c$.

All dynamical properties of the TLS can be obtained from the 2 \times 2 RDM.

$$\tilde{\rho}_{\alpha''\alpha'}(t) = \operatorname{Tr}_{\text{bath}} \langle \alpha'' | e^{-i\hat{H}t/\hbar} \hat{\rho}(0) e^{i\hat{H}t/\hbar} | \alpha' \rangle \tag{2.7}$$

where α' , $\alpha'' = R$, L. As usual, we assume that the initial density operator is a product of system and bath components,

$$\hat{\rho}(0) = \hat{\rho}_{\text{sys}}(0)\hat{\rho}_{\text{bath}}(0), \tag{2.8}$$

and $\hat{\rho}_{\rm bath}(0)=e^{-\beta\hat{H}_{\rm bath}^{\rm free}}\Big/{\rm Tr}e^{-\beta\hat{H}_{\rm bath}^{\rm free}}$ (where $\beta=1/k_{\rm B}T$ is the inverse temperature) is the Boltzmann operator for the free bath Hamiltonian, given by eqn (2.3) with $c_i = 0$.

(ii) Populations, coherences and purity

If the RDM can be expressed in terms of a single state, the purity is equal to unity and the von Neumann entropy is equal to zero. If, on the other hand, Q < 1 or S > 0, the RDM represents a mixture. In the case of a TLS, the purity is given by

$$Q = \tilde{\rho}_{RR}^2 + \tilde{\rho}_{LL}^2 + 2|\tilde{\rho}_{RL}|^2 = 1 - 2(\tilde{\rho}_{RR}\tilde{\rho}_{LL} - \tilde{\rho}_{RL}\tilde{\rho}_{RL}^*).$$
(2.9)

Regardless of the system's initial preparation, the site populations eventually attain the same value,

$$\lim_{t \to \infty} \tilde{\rho}_{RR} = \lim_{t \to \infty} \tilde{\rho}_{LL} = \frac{1}{2}.$$
 (2.10)

Further, the imaginary part of the off-diagonal element is related to the time derivative of a site population.²³ This is easily seen by differentiating the RDM and evaluating the commutator for the system-bath Hamiltonian:

$$\frac{\mathrm{d}}{\mathrm{d}t}\tilde{\rho}_{\mathrm{RR}}(t) = \frac{i}{\hbar}\mathrm{Tr}\Big(e^{-i\hat{H}t/\hbar}\hat{\rho}(0)e^{i\hat{H}t/\hbar}\big[\hat{H},|\mathrm{R}\rangle\langle\mathrm{R}|\big]\Big) = 2\Omega\mathrm{Im}\,\tilde{\rho}_{\mathrm{RL}}(t). \tag{2.11}$$

It follows that the imaginary part of $\tilde{\rho}_{RL}$ always vanishes at equilibrium, i.e.,

$$\lim_{t \to \infty} \operatorname{Im} \tilde{\rho}_{RL} = 0. \tag{2.12}$$

According to eqn (2.9), the purity is equal to unity if $\tilde{\rho}_{RL}\tilde{\rho}_{RL}^*$ = $\tilde{\rho}_{RR}\tilde{\rho}_{LL}$. From eqn (2.10) and (2.12), a perfect recovery of purity at long times would be possible if

$$\lim_{t \to \infty} \tilde{\rho}_{RL} = \lim_{t \to \infty} \tilde{\rho}_{LR} = \pm \frac{1}{2}.$$
 (2.13)

Thus, we see that a complete recovery of purity is realizable if the RDM approaches the form

$$\lim_{t \to \infty} \hat{\hat{\rho}}(t) = \frac{1}{2} (|R\rangle\langle R| + |L\rangle\langle L|) \pm \frac{1}{2} (|R\rangle\langle L| + |L\rangle\langle R|). \quad (2.14)$$

According to eqn (2.2), this condition for the RDM is equivalent to one of the following two possibilities,

$$\lim_{t \to \infty} \hat{\tilde{\rho}}(t) = |\Phi_0\rangle \langle \Phi_0| \text{ or } \lim_{t \to \infty} \tilde{\rho}(t) = |\Phi_1\rangle \langle \Phi_1|. \tag{2.15}$$

Not surprisingly, eqn (2.15) states that perfect purity at long times is possible if the TLS approaches one of its two

eigenstates. Since the excited state is not thermodynamically reachable at equilibrium, we conclude that a full recovery of purity requires

$$\lim_{t \to \infty} \hat{\hat{\rho}}(t) = |\Phi_0\rangle \langle \Phi_0|. \tag{2.16}$$

To achieve perfect purity at long time, the dissipative TLS must occupy the ground state of the bare TLS. This seems possible in the limit of zero temperature and vanishingly small system-bath coupling.

Next, according to eqn (2.9),

$$\operatorname{Tr}\tilde{\rho}^2 \ge Q_{\mathrm{incoh}}$$
 (2.17)

where

$$Q_{\text{incoh}} \equiv \tilde{\rho}_{RR}^2 + \tilde{\rho}_{LL}^2 = 2\left(\tilde{\rho}_{RR} - \frac{1}{2}\right)^2 + \frac{1}{2}.$$
 (2.18)

The function Q_{incoh} is a fully incoherent contribution that provides a lower bound to the value of purity. Its minimum value, equal to $\frac{1}{2}$ (which corresponds to a maximally mixed state), occurs at $\tilde{\rho}_{RR} = \frac{1}{2}$. We emphasize that eqn (2.18) is only a lower bound to the total purity, and the population value $\tilde{\rho}_{RR} = \frac{1}{2}$ corresponds to a fully mixed state only if $\tilde{\rho}_{RL} = 0$. Thus the purity of a TLS is bounded by the inequalities

$$\frac{1}{2} \le \operatorname{Tr}\tilde{\rho}^2 \le 1. \tag{2.19}$$

According to eqn (2.9), the purity of a symmetric TLS is a function of two RDM elements, $\tilde{\rho}_{RR}$ and $|\tilde{\rho}_{RL}|$, and is given by the expression

$$Q = 2\left(\tilde{\rho}_{RR} - \frac{1}{2}\right)^2 + 2|\tilde{\rho}_{RL}|^2 + \frac{1}{2}.$$
 (2.20)

The purity is plotted in Fig. 1 as a function of the diagonal and the magnitude of the off-diagonal RDM element. Note that eqn (2.20) also provides an upper limit for the magnitude of the

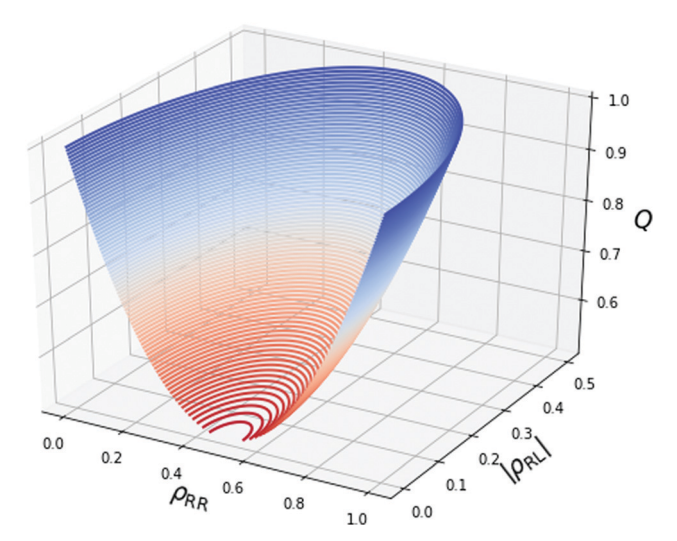


Fig. 1 Plot of the purity as a function of the diagonal and off-diagonal

RDM off-diagonal element,

$$|\tilde{\rho}_{RL}| \le \sqrt{\tilde{\rho}_{RR}(1 - \tilde{\rho}_{RR})}.$$
 (2.21)

According to eqn (2.9), in the case of a symmetric TLS the site population $\tilde{\rho}_{RR}=\frac{1}{2}$ of a maximally mixed state implies $\tilde{\rho}_{RL}=0$. Thus, the RDM associated with a fully mixed state has the form

$$\lim_{t \to \infty} \tilde{\rho}(t) = \frac{1}{2} (|R\rangle\langle R| + |L\rangle\langle L|), \tag{2.22}$$

which may also be written in terms of the TLS eigenstates as

$$\lim_{t \to \infty} \tilde{\rho}(t) = \frac{1}{2} (|\Phi_0\rangle \langle \Phi_0| + |\Phi_1\rangle \langle \Phi_1|). \tag{2.23}$$

Eqn (2.23) states that a complete loss of purity is associated with a mixture of the ground and excited TLS eigenstates, with equal coefficients. When the process has reached equilibrium, this situation corresponds to infinite temperature. An interesting question is whether a system can temporarily attain a fully mixed state, but subsequently recover and eventually evolve to a state of higher purity. The calculations presented in the next section and in Paper Π^{24} explore this question with regard to tunneling and relaxation dynamics.

In our recent work¹⁸ we showed that the second term in eqn (2.20), the square of the off-diagonal RDM element, can be rewritten in terms of two physically meaningful contributions,

$$2|\tilde{\rho}_{\rm RL}|^2 = Q_{\rm pop-dif}(t) + Q_{\rm t-der}(t). \tag{2.24}$$

The first term in this expression is given by the squared difference of the TLS eigenstate populations,

$$Q_{\text{pop-dif}}(t) \equiv \frac{1}{2} (\tilde{\rho}_{00}(t) - \tilde{\rho}_{11}(t))^2,$$
 (2.25)

while, according to eqn (2.11), the other term is proportional to the square of the time derivative of a site population,

$$Q_{\text{t-der}}(t) \equiv \frac{1}{2} \Omega^{-2} \dot{\hat{\rho}}_{RR}(t)^2,$$
 (2.26)

Thus the total purity is the sum of three terms,

$$Q(t) = Q_{\text{incoh}}(t) + Q_{\text{pop-dif}}(t) + Q_{\text{t-der}}(t).$$
 (2.27)

Eqn (2.27) was derived ref. 18 in order to explain the interesting purity patterns that emerged from our path integral calculations.

A great deal regarding the dynamics of purity can be deduced based on simple considerations for the evolution of these contributions. As discussed earlier, $Q_{\rm incoh}$ is a fully incoherent term that tends to dominate under strongly dissipative, high-temperature conditions. The population difference term is expected to be small at high temperature and approach $\frac{1}{2}$ in the low-temperature, weakly dissipative regime. The time derivative term can be large when the site populations exhibit oscillatory dynamics. Last, symmetry relations can cause these terms to be preserved or to vanish. These situations are discussed in the next two sections in the context of tunneling dynamics, and in Paper II in the case of eigenstate initial conditions.

III. Purity during tunneling dynamics

When prepared in a localized state,

$$\hat{\rho}_{\text{svs}}(0) = \tilde{\rho}(0) = |\mathbf{R}\rangle\langle\mathbf{R}|, \tag{3.1}$$

an isolated symmetric TLS will execute fully coherent tunneling oscillations. Contact with a dissipative bath introduces dephasing and population transfer, which leads to a gradual loss of coherence. Depending on the various parameters (and excluding the localization transition²), the site populations of a symmetric TLS may then display underdamped oscillations or a featureless decay, eventually reaching equilibrium.

The two RDM elements entering eqn (2.20), $\tilde{\rho}_{RR}$ and $|\tilde{\rho}_{RL}|$, are connected through the dynamics. An interesting question concerns what portion of the accessible space (shown in Fig. 1) of these variables is actually visited during the time evolution of a TLS. This question is investigated in detail in the next section through numerical calculations. Interestingly, as we show in Paper II, ²⁴ symmetry considerations lead to an entirely different situation when the TLS is initially prepared in one of its eigenstates.

Eqn (2.20) may be used to deduce the early-time behavior of purity. Taking the time derivative, we find

$$\frac{\mathrm{d}Q}{\mathrm{d}t} = \frac{\mathrm{d}}{\mathrm{d}t} \left(1 + 2\tilde{\rho}_{\mathrm{RR}}^{2} - 2\tilde{\rho}_{\mathrm{RR}} + 2|\tilde{\rho}_{\mathrm{RL}}|^{2} \right)
= 4\tilde{\rho}_{\mathrm{RR}} \frac{\mathrm{d}\tilde{\rho}_{\mathrm{RR}}}{\mathrm{d}t} - 2\frac{\mathrm{d}\tilde{\rho}_{\mathrm{RR}}}{\mathrm{d}t} + 4|\tilde{\rho}_{\mathrm{RL}}| \frac{\mathrm{d}|\tilde{\rho}_{\mathrm{RL}}|}{\mathrm{d}t}.$$
(3.2)

Using the relation²³

$$\frac{\mathrm{d}\tilde{\rho}_{\mathrm{RR}}}{\mathrm{d}t} = 2\Omega \mathrm{Im}\,\tilde{\rho}_{\mathrm{RL}},\tag{3.3}$$

we see that for any real-valued initial RDM, $\dot{\tilde{\rho}}_{RR}(0) = 0$. Thus the linear term in a time expansion of the site population vanishes, implying that the population evolution is quadratic (or higher-order) at short times. Since the off-diagonal RDM element is zero for the tunneling initial condition, eqn (3.2) leads to

$$\dot{Q}(0) = 0, \tag{3.4}$$

which implies that the purity is also quadratic at short times. Starting with a pure state, the purity always decreases initially, thus we conclude that the short time behavior of purity during tunneling dynamics is Gaussian. This result is consistent with the conclusions of earlier work based on power series expansions²¹ and perturbative treatments.^{13,15–17} However, we show in Paper II that under different initial conditions the short-time behavior of purity can be non-Gaussian and even increasing.

For a localized initial state, $\tilde{\rho}_{RR}(0) = 1$, Q_{incoh} is initially equal to unity and begins to decrease as soon as the site populations change in value. Eventually, the site populations reach $\frac{1}{2}$, thus the sum of the squared site populations approaches the maximally mixed value $\frac{1}{2}$.

The population difference term $Q_{\rm pop-dif}$ vanishes at t=0 for an initially localized TLS state, as $\tilde{\rho}_{00}(0)=\tilde{\rho}_{11}(0)=\frac{1}{2}$. As time

progresses, population begins to transfer from the excited to the ground state, until the two populations attain the Boltzmann relation (projected onto the TLS subspace), thus the population difference term rises gradually during tunneling dynamics and may lead to a rebound of purity. The instantaneous rate term Q_{t-der} depends strongly on the parameter regime. This terms starts at zero in the case of a localized initial state and grows slightly, but not much, in the overdamped regime characterized by a slow population decay. However, low-temperature, weakly dissipative conditions give rise to oscillatory population dynamics which can lead to large-amplitude oscillatory behavior of $\tilde{\rho}_{RR}$, and thus of $Q_{\text{t-der}}$. The contribution from this large term can counter early on the decay resulting from the incoherent term. These behaviors are observed and discussed in the next section.

Further, it is insightful to analyze the time evolution of purity in the context of the dissipative processes that lead to decoherence of the TLS. In the path integral representation 25,26 of the RDM, the effects of the bath enter through the Feynman-Vernon influence functional, 27 which is given by a Gaussian expression in terms of the coordinates of the TLS paths. Earlier work²⁰ has identified two contributions to decoherence. The first is a classical contribution associated with the dephasing effects from the fluctuating TLS site energies.²⁰ This term is dominant in the case of strongly dissipative, sluggish baths at high temperature. Its coherence-quenching effects arise from phonon absorption and stimulated emission, according to a mechanism reminiscent of light-matter interactions.²⁰ The memory associated with the classical decoherence mechanism is fully removable.28,29

The second contribution to decoherence is associated with a strictly quantum mechanical process that involves spontaneous phonon emission.²⁰ The memory effects from this quantum contribution to decoherence are linked to the "back-reaction" and are not removable.²⁹ As expected based on its spontaneous emission nature, the quantum contribution to decoherence is important primarily at low temperatures. This mechanism is entirely responsible for detailed balance,29 and thus for the eigenstate population difference term $Q_{pop-dif}$.

IV. Path integral results during tunneling dynamics

In this section we investigate the time evolution of purity during the tunneling dynamics of a symmetric TLS coupled to a model harmonic bath. The initial density operator corresponds to the right-localized state given in eqn (3.1). Numerically exact results for the time evolution of the RDM are obtained through a combination of the iterative quasiadiabatic propagator path integral^{30–32} (QuAPI) methodology, along with its blip decomposition^{33,34} and the small matrix disentanglement of the path integral^{35,36} (SMatPI) which eliminates the tensor storage requirement of the QuAPI algorithm. These methods are numerically exact once converged with respect to the path integral time step and the included memory length, and are applicable to dissipative baths characterized by completely general spectral density functions, which may correspond to simple analytical models or may describe solvent or biological environments.

(i) Dependence of purity dynamics on dissipation strength

To elucidate the effect of system-bath coupling strength on the long time behavior of purity, we focus on the low-temperature regime where a variety of behaviors are observed. Fig. 2 shows the dependence of purity on dissipation strength for a TLS coupled to a low-temperature bath characterized by $\hbar\Omega\beta = 10$ and $\omega_c = 5\Omega$. The low effective bath temperature of $\hbar\omega_c\beta = 50$ causes the majority of excited system-bath states to be inaccessible, and with sufficiently weak system-bath coupling the equilibrium RDM is dominated by the TLS ground state. This implies that the long-time value of purity can approach unity in this regime. However, its transient dynamics can exhibit strongly nonmonotonic behavior. As seen in Fig. 2, the purity decreases rapidly at early times, falling to a minimum value and subsequently recovering for some of the parameters. The partial decay of purity spans a time much shorter than the span of the oscillatory population dynamics, which are associated with quantum coherence. The subsequent revival is seen to be nearly complete

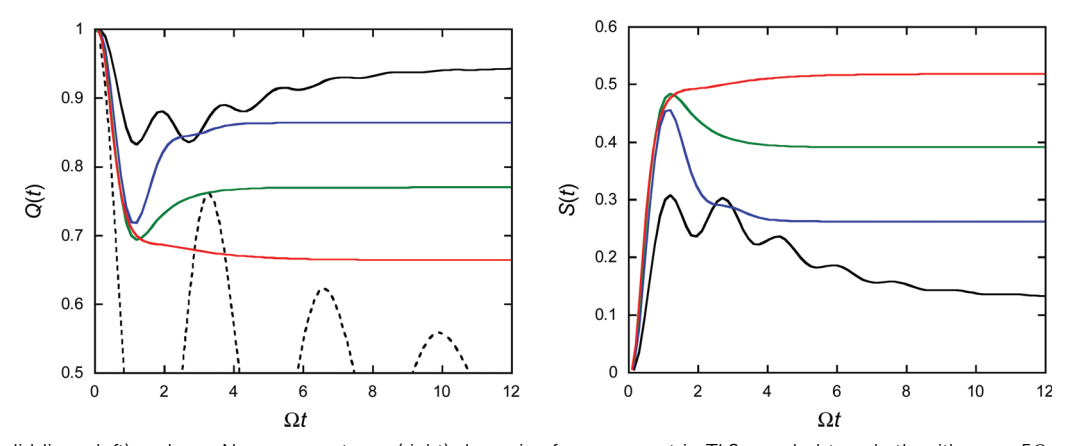


Fig. 2 Purity (solid lines, left) and von Neumann entropy (right) dynamics for a symmetric TLS coupled to a bath with $\omega_c = 5\Omega$ at $\hbar\Omega\beta = 10$ from converged path integral calculations. Black, blue, green and red curves (purity: top-to-bottom, entropy: bottom to top): $\xi = 0.1$, 0.3, 0.5 and 0.7. The dashed black line shows the population of the initial state, $\rho_{RR}(t)$

at small values of the Kondo parameter and partial at intermediate values. As the dissipation strength grows, the entanglement of system and bath states increases, leading to a less pronounced recovery of purity. No rebound is observed under strongly dissipative conditions, and purity then decays monotonically to its equilibrium value.

Also shown in Fig. 2 is the time evolution of the von Neumann entropy. Consistent trends are observed, i.e. the TLS entropy increases monotonically in the strong dissipation regime but decreases subsequent to its early rise when the system-bath coupling is weak.

(ii) Temperature dependence of purity dynamics

Fig. 3 shows the effect of temperature on the time evolution of purity for $\omega_c = 5\Omega$ with an intermediate value of the system-bath coupling strength, $\xi = 0.3$ and $\lambda = 3\hbar\Omega$. The most pronounced recovery of purity is observed at the lowest temperature. The non-monotonic evolution disappears when the temperature becomes approximately equal to the TLS tunneling splitting, and a continuous decay of purity is observed at higher temperatures. At the highest temperature of $\hbar\Omega\beta$ = 0.1 the purity decays monotonically to an almost fully mixed state. The von Neumann entropy displays similar trends, reaching a local maximum at low temperatures followed by a significant decrease.

(iii) Dependence of purity on bath time scale

Next, we examine the effects of varying the frequency composition of the bath. For this study we vary the Kondo parameter in order to maintain a constant reorganization energy. The path integral results for the time evolution for purity and entropy are shown in Fig. 4. It is seen that the purity dynamics depends significantly on the value of the bath cutoff frequency. The most pronounced recovery of purity is observed with large values of ω_c , for which the majority of bath oscillators remain in their ground state. An interesting behavior is observed at small ω_c values, which correspond to a nearly classical bath. In this regime the purity begins to rise after reaching its minimum value, but quickly falls somewhat prior to stabilizing.

(iv) Memory effects

Memory effects tend to be more prominent when the bath is composed primarily of slow degrees of freedom, i.e. when ω_c Ω , as the bath correlation function tends to decay slowly in such cases. With the large bath cutoff frequency of the parameter set in Fig. 2, memory effects on the population dynamics tend to be moderate. However, Fig. 5 shows that bath-induced memory plays a crucial role to the recovery of purity at low temperature. When a memory is truncated to short lengths in the calculation, purity always shows a downward behavior, attaining a long-time value close to $\frac{1}{2}$, which is far from being correct when the systembath coupling strength is small. As the memory length $\tau_{\rm m}$ included in the calculation increases, purity rebound in the small coupling regime becomes noticeable, eventually converging to the nearly complete recovery value observed in Fig. 5 under weakly dissipative conditions.

(v) Physically meaningful contributions to purity dynamics

The three contributions to purity discussed in the previous section are shown in Fig. 6 for small and moderate values of the system-bath coupling. In this regime the incoherent term Q_{incoh} displays an oscillatory pattern which follows the oscillations of the site populations. The term $Q_{\text{pop-dif}}$, which is associated with the difference of the eigenstate populations, rises steadily to its maximum value, which can approach $\frac{1}{2}$ at this low temperature. This term is responsible for the long-time recovery of purity.

Under weakly dissipative conditions, the third term, $Q_{t\text{-der}}$ exhibits oscillatory evolution, attaining relatively large values early on, which result from the rapid, large-amplitude oscillation of the site populations. As seen in Fig. 6, the magnitude of this term opposes the drop of purity from the Q_{incoh} term, preventing a significant decrease at early times. Thus, the complex interplay among the three contributions given in eqn (2.27) lead to the observed non-monotonic evolution of purity. In particular, the combination of $Q_{pop-dif}$ and Q_{t-der} allows purity to sustain a relatively high value throughout the dynamics.

Also shown in Fig. 6 is the contribution to these terms from the classical decoherence process associated with level

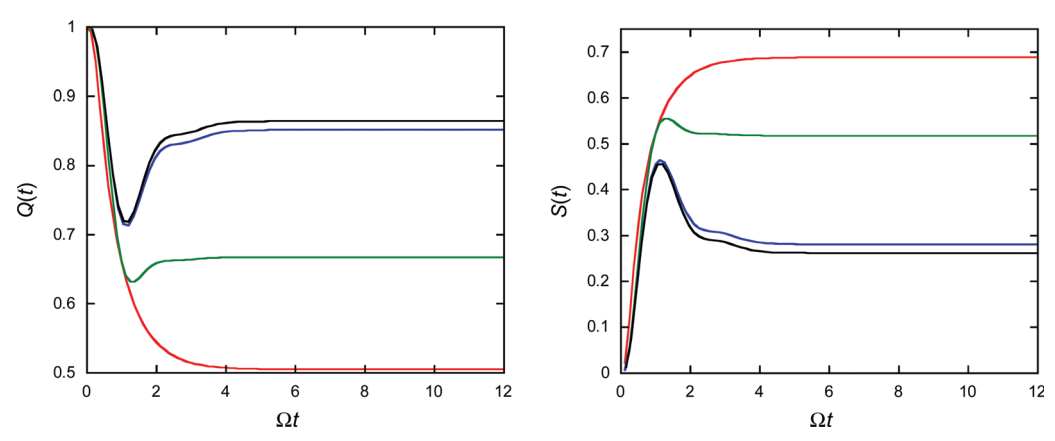


Fig. 3 Purity (left) and von Neumann entropy (right) dynamics for a symmetric TLS coupled to a bath with $\xi = 0.3$ and $\omega_c = 5\Omega$ from converged path integral calculations. Black, blue, green and red curves (purity: top-to-bottom, entropy: bottom to top): $\hbar\Omega\beta$ = 10, 5, 1 and 0.1.

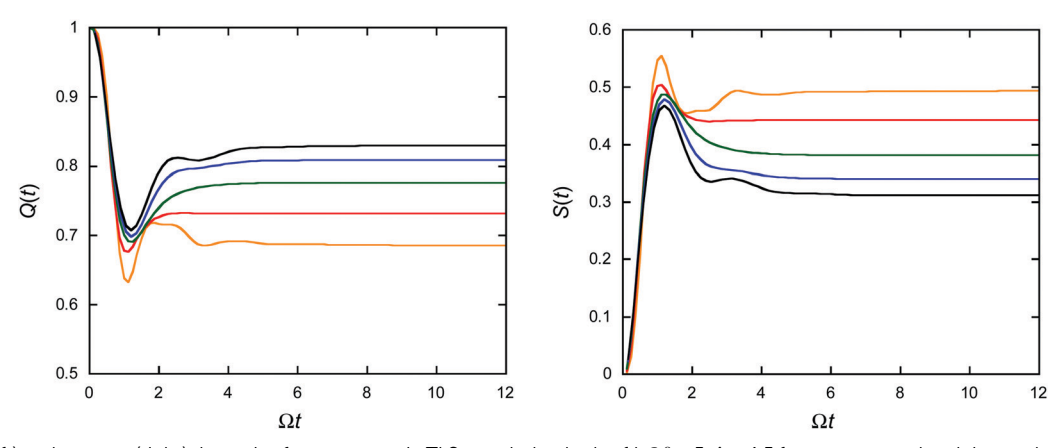


Fig. 4 Purity (left) and entropy (right) dynamics for a symmetric TLS coupled to bath of $\hbar\Omega\beta = 5$, $\lambda = 4.5$ from converged path integral calculations. Black, blue, green, red and orange curves (purity: top-to-bottom, entropy: bottom to top): $\omega_c = 10\Omega$, $\xi = 0.225$; $\omega_c = 7.5\Omega$, $\xi = 0.3$; $\omega_c = 5\Omega$, $\xi = 0.45$; $\omega_c = 2.5\Omega$, ξ = 0.9; and $\omega_{\rm c}$ = 1.25 Ω , ξ = 1.8, respectively.

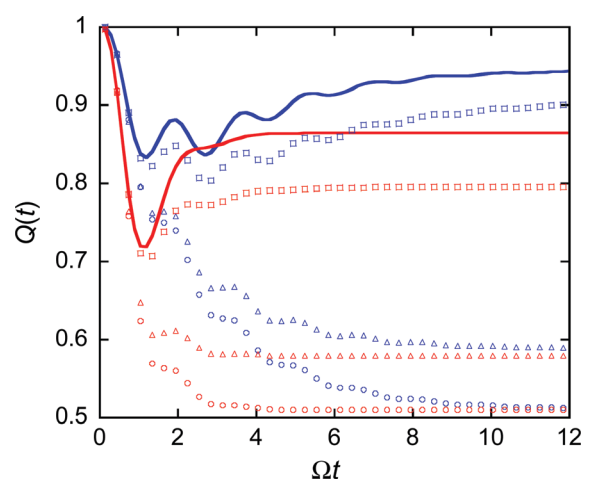


Fig. 5 Memory effects on purity dynamics for a symmetric TLS coupled to bath of $\omega_{\rm c}$ = 5Ω at $\hbar\Omega\beta$ = 10. Solid lines: exact path integral results. Circles, triangles and squares are unconverged results obtained with $\Omega \tau_{\rm m}$ = 0.15, 0.3 and 0.6. Blue (higher values): ξ = 0.1. Red (lower values): ξ = 0.3.

fluctuations driven by the bath, which lead to energy exchange in the form of phonon absorption and stimulated emission. It is seen that this classical mechanism captures almost quantitatively the incoherent contribution to purity, Q_{incoh} , as well as the time-derivative contribution Q_{t-der} . However, this classical process is unable to account for detailed balance, thus it fails to reproduce the rise of the population difference component $Q_{\text{pop-dif}}$. As a result, the classical decoherence mechanism alone fails to account for the recovery of purity. Thus, it is seen that purity recovery involves a strictly quantum mechanical decoherence process associated with spontaneous phonon emission. The latter is required for the cooling the TLS.

(vi) Flow of RDM elements

The analysis presented in Section II showed that in the case of a symmetric TLS purity depends on two variables, the population of a TLS site and the magnitude of the off-diagonal element. The relation between these two variables is determined by the dynamics, and the possible spread of the $(\tilde{\rho}_{RR}, |\tilde{\rho}_{RL}|)$ pairs is bounded by eqn (2.21). For each such pair, the value of purity is given by eqn (2.20).

Fig. 7 shows the spread of the RDM pairs $(\tilde{\rho}_{RR}, |\tilde{\rho}_{RL}|)$, along with the corresponding value of purity for four parameters sets. The initial point (1,0) has Q = 1 and thus lies on the boundary of the purity region. As time progresses the purity begins to drop, thus the pair begins to move toward the interior of the allowed region.

With weakly dissipative, low-temperature parameters, the RDM pairs follow a ribbon-like curve that intersects itself a few times, eventually stabilizing at the equilibrium value $(\frac{1}{2}, (\text{Re}\tilde{\rho}_{\text{RL}})^2)$ which lies near the boundary of the accessible region, as the equilibrium purity value is close to unity in this regime. By contrast, the evolution becomes less complex as the site population dynamics becomes less oscillatory. Under strongly dissipative conditions and high temperature, the RDM pairs quickly turn toward the central, low-purity region without recrossing. In all cases, the bulk of the interior is not accessed by the dynamics.

V. Purity during excitation energy transfer in the bacteriochlorophyll dimer

To assess the relevance of these behaviors to real molecular systems, we investigate in this section the evolution of purity during the dynamics of excitation energy transfer (EET) in the bacteriochlorophyll (BChl) dimer. This system is of interest because of its role in the solar energy capture by photosynthetic bacteria.³⁷ In the BChl dimer energy flows between the singly excited electronic states of a BChl pair, where the two molecules, each with its own intramolecular vibrations, interact through Frenkel exciton terms³⁸⁻⁴⁰ with a calculated coupling constant $I = 363 \text{ cm}^{-1}.^{41}$

The nature of the EET in BChl aggregates has been under intense debate, 42-45 primarily with regard to the possibility of **Paper**

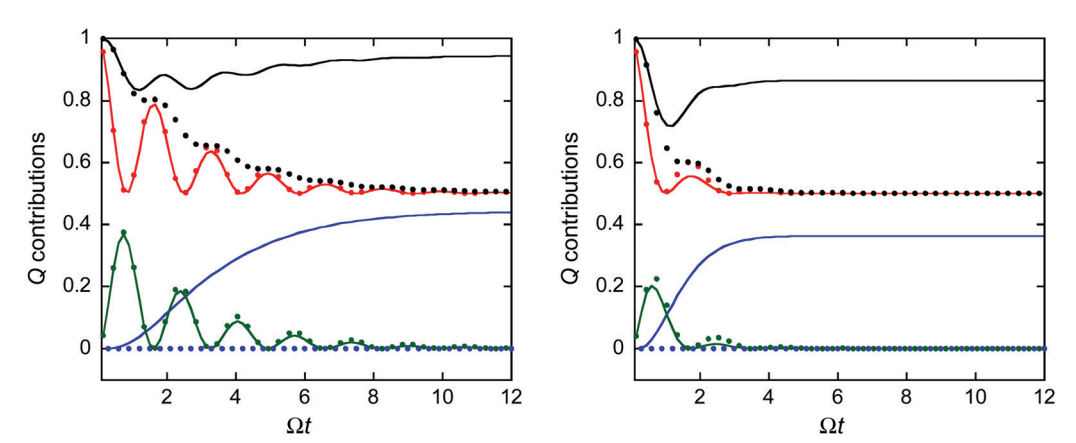


Fig. 6 Contributions to TLS purity dynamics at a low temperature, $\hbar\Omega\beta$ = 10, ω_c = 5 Ω . Black, red, blue and green lines (top to bottom at long times) show the total purity and the Q_{incoh} , $Q_{\text{pop-dif}}$ and $Q_{\text{t-der}}$ terms, respectively. Red, blue and green circles show the contribution to these terms from the classical decoherence mechanism. The black circles show the total classical contribution to the purity. Left: $\xi = 0.1$. Right: $\xi = 0.3$.

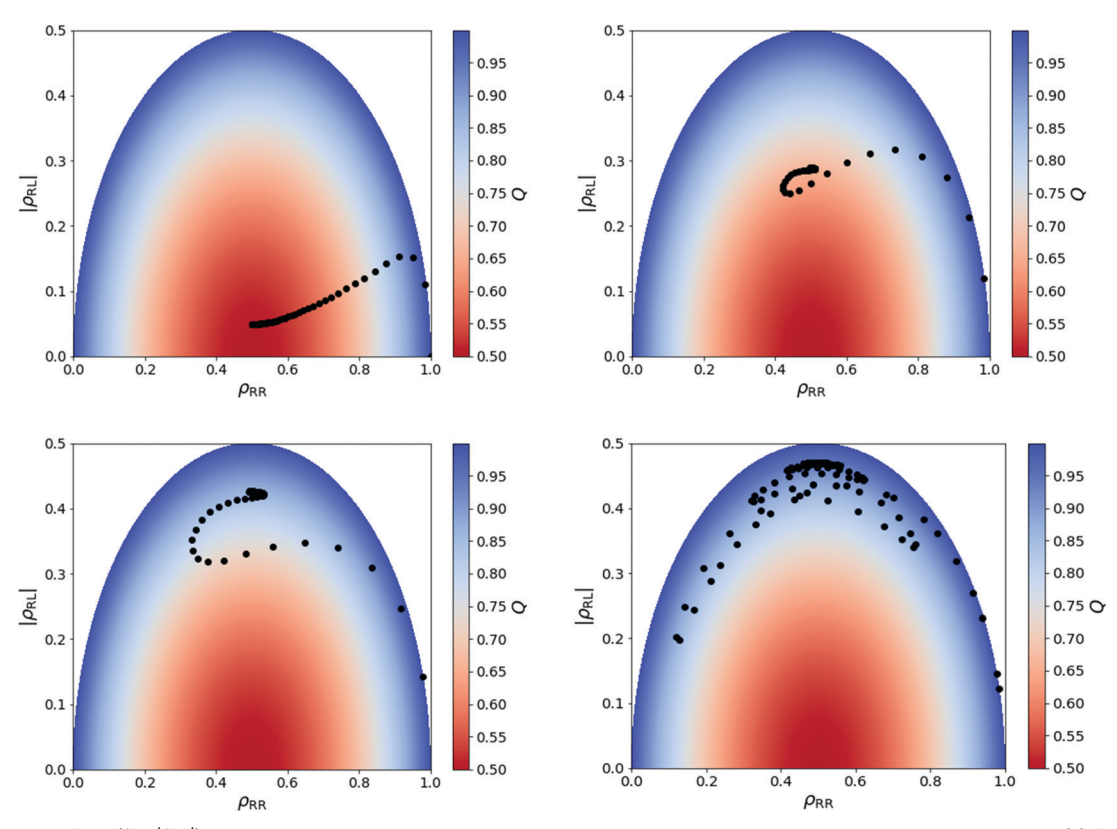


Fig. 7 Exploration of the $(\tilde{\rho}_{RR},|\tilde{\rho}_{RL}|)$ space during the RDM dynamics. The color map corresponds to the purity value at each point. (a) $\xi = 0.3$, $\omega_c = 5\Omega$, $\hbar\Omega\beta=0.1\text{, (b) }\xi=0.3\text{, }\omega_{\text{c}}=5\Omega\text{, }\hbar\Omega\beta=1\text{, (c) }\xi=0.3\text{, }\omega_{\text{c}}=5\Omega\text{, }\hbar\Omega\beta=10\text{, (d) }\xi=0.1\text{, }\omega_{\text{c}}=5\Omega\text{, }\hbar\Omega\beta=10\text{.}$

electronic coherence and the role of vibrations in oscillatory patterns⁴⁶⁻⁴⁹ identified through fluorescence anisotropy and two-dimensional spectroscopic techniques. 50-52 Recent work 53 suggested the use of two-dimensional wavepacket interferometry as a probe of electronic coherence in the dimer. Even though the parameters of 50 vibrational BChl modes with nonzero Huang-Rhys factors are available from high-resolution spectroscopic experiments,54 the vast majority of theoretical studies have relied on calculations based on one or two vibrational degrees of freedom, all-mode treatments of exciton-vibration dynamics using approximate treatments, or non-perturbative calculations on simplified spectral density models (see ref. 55-57 and references therein).

Our group recently reported numerically exact path integral simulations of EET dynamics in the BChl dimer58 and in aggregates containing up to 19 pigments,59 where the excitonvibration dynamics resulting from all 50 vibrational modes in each pigment were treated fully quantum mechanically at room

temperature. In the case of the BChl dimer, it was shown⁵⁸ that a coordinate transformation maps the exciton-vibration Hamiltonian on a TLS where both states are coupled to a common vibrational bath with rescaled coupling coefficients. The populations of the singly excited electronic states were obtained using the quantum-classical path integral (QCPI) methodology^{60,61} with dynamically consistent state hopping⁶² (DCSH) and the harmonic treatment of the back reaction 63,64 (HBR), which yields fully quantum mechanical results when the system's environment is given by a quadratic Hamiltonian, while maintaining a constant number of trajectories (i.e. scales as a typical molecular dynamics calculation). The dimer populations were seen to exhibit underdamped oscillations of a moderate amplitude. Calculations on much longer aggregates were performed with the modular decomposition of the path integral^{65–68} (MPI), which is characterized by linear scaling with the number of molecular units. The MPI calculations showed that the large-amplitude electronic recurrences observed in the dimer are rapidly quenched in long BChl aggregates.⁵⁹

In Fig. 8 we compare QCPI and SMatPI results for the time evolution of purity in the BChl dimer at 300 K. The 50 vibrational modes are initially equilibrated with respect to the ground electronic state of each pigment, in accordance with a Franck-Condon excitation. Once converged, both methods produce numerically exact results. In the case of the BChl dimer, the discrete vibrational modes induce a very long-lived memory. The QCPI methodology automatically (i.e. without path integral time slicing) captures all the classical memory associated with stimulated phonon events,61 and (through DCSH) some of quantum memory as well. For this reason the OCPI calculation converges faster with respect to the memory treated explicitly. The full path integral treatment of the system-bath interaction ensures that the converged populations obey the detailed balance condition. 60,61 However, the SMatPI decomposition allows the treatment of longer memory, leading to converged and stable results over long times. As seen in Fig. 8, the results obtained with the two methods are in good agreement within the Monte Carlo error of the QCPI calculation (with 150 000 initial condition samples per integration variable). We emphasize again that the purity, a quantity that depends on the squares of diagonal and off-diagonal RDM elements, is very sensitive to memory and requires highly accurate calculations.

The evolution of purity during the excitation energy transfer dynamics of the BChl dimer is seen to be similar to that observed in the low-temperature, weak dissipation models examined in the previous section. An attempt to estimate the decoherence time from the initial decay of purity would lead to the incorrect conclusion that quantum coherence is quenched within approximately 20 fs. However, one sees from Fig. 8 that large amplitude oscillations in the population of the excited BChl molecule persist for more than 200 fs.

Also shown in Fig. 8 are the contributions from the incoherent, population difference and time derivative terms. The incoherent contribution reaches its minimum value early on and oscillates around its equilibrium value of 0.5. The population-difference term reaches a moderately high value

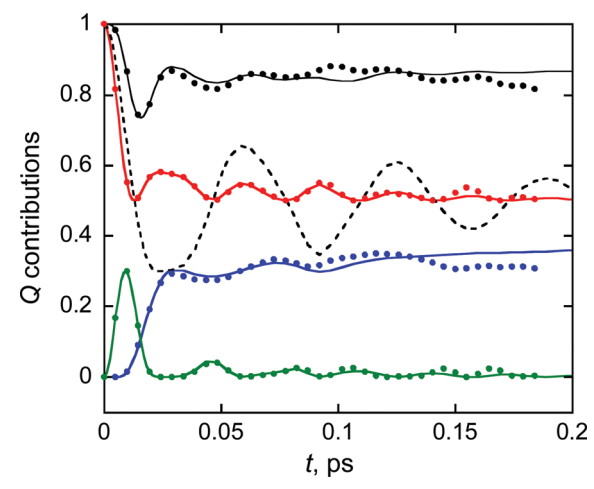


Fig. 8 Contributions to purity in BChl exciton-vibration dynamics with Franck-Condon initial condition. Markers: QCPI results. Lines: SMatPI results. Black, red, blue and green (top to bottom) solid lines and markers show the total purity and the Q_{incoh} , $Q_{\text{pop-dif}}$ and $Q_{\text{t-der}}$ terms, respectively. The dashed black line shows the population of the initially excited BChl molecule obtained from the SMatPI calculation

of 0.3 that eventually sustains the purity around 0.83. The time derivative contribution exhibits an initial jump owing to the large-amplitude site oscillations, which keeps the purity from dropping significantly early on, when the population difference is still quite small. As a result, the total purity drops to its minimum value of 0.74 around 15 fs, and subsequently recovers to a considerably high equilibrium value of 0.86. These results show that the recovery of purity can be observed in actual molecular systems under physiological conditions.

VI. Concluding remarks

The evolution of purity in a symmetric TLS coupled to a dissipative harmonic bath can display complex behaviors. Through a general theoretical analysis we established bounds and some general constraints. The behaviors discussed in Section II are valid with any initial condition. The remaining of this paper focused on the purity of a TLS undergoing dissipative tunneling dynamics. In this case we used simple arguments to show in Section III that the initial decay of purity is quadratic in time.

In Sections II and III we also discussed the role of various physical processes on the dynamics of purity. We showed that under high-temperature, strongly dissipative conditions, which give rise to monotonic population decay, the purity is dominated by the incoherent term given by the sum of the squared site populations, which decays to the lowest possible value of purity associated with a maximally mixed RDM. As the temperature is lowered, a second contribution, which arises from the population difference of the TLS eigenstates, becomes increasingly important as time progresses and dominates the purity value at long times. When the equilibrium Boltzmann factor reflects a significant population difference, the long-time value of purity can approach unity. This implies that purity reaches a

minimum at intermediate times, after which it rises again. A third contribution to purity is associated with the time derivative of site populations. Under weakly dissipative conditions which lead to underdamped population dynamics, this term introduces a large oscillatory contribution to purity which is most important at short to intermediate times and which increases the minimum value of purity, maintaining a relatively high value throughout the course of dynamics.

This analysis was supported and quantified through numerically exact real-time path integral calculations. The results presented in Sections IV and V showed that the recovery of purity can be substantial in the low-temperature, weak-dissipation regime, and examined the effects of dissipation strength, temperature, and the time scale of the bath on purity dynamics. Purity recovery was also observed in the excitation energy transfer within a BChl dimer at room temperature, showing that this effect is not expected only in model systems under unrealistic conditions. The path integral calculations also revealed the emergence of a new nonmonotonic behavior in the strong dissipation regime caused by a slow bath.

Memory effects induced by the bath play a very important role in the evolution of purity, in particular with regard to its recovery. Early truncation of the length of memory terms included in the path integral calculations prevents the rebound of purity, leading to a steady decline. The purity is considerably more sensitive to memory than the site populations.

We also discussed the effects on purity dynamics arising from the two distinct decoherence mechanisms associated with stimulated and spontaneous phonon processes. The former, classical decoherence process is the dominant contribution to the incoherent and the time derivative purity terms, as it is associated with the dephasing effects from site level fluctuations. On the other hand, spontaneous phonon emission is intimately linked to the detailed balance property and thus to the eigenstate population difference reached at long times. As a result, this strictly quantum mechanical mechanism is responsible for the long-term recovery of purity at low temperatures.

The non-monotonic evolution of purity in some regimes and its nearly quantitative recovery when the TLS dynamics has settled to the RDM equilibrium values imply that the value of purity is not necessarily indicative of coherence or its loss. Examination of the numerical results presented in Sections IV and V reveals that the purity can be at its minimum value early on, when the population dynamics is highly oscillatory. An attempt to deduce the decoherence time from the early dynamics of purity, under the assumption that the purity would continue to decay, would lead to the incorrect prediction of very short-lived coherence. This situation was illustrated very clearly in the case of excitation energy transfer in the BChl dimer shown in Fig. 8, where the initial decay of purity spans just 20 fs, while coherent oscillations persist for over 200 fs. Further, the purity may reach a value indicative of a nearly pure RDM after all dynamics has ended. This is the case when the equilibrium RDM is dominated by the ground state of the TLS. While the ground eigenstate is a coherent superposition of the two localized states, coherence in the context of dynamics is associated with quantum beats which, in the case of a TLS, correspond to

population exchange between right- and left-localized states. Such population transfer ceases completely once the system reaches equilibrium. Both of these observations suggest that the purity of the RDM should not be used as a measure of decoherence in the dynamics of quantum dissipative systems.

Conflicts of interest

There are no conflicts of interest to declare

Acknowledgements

This material is based upon work supported by the National Science Foundation Center for Synthesizing Quantum Coherence under Grant No. 1925690.

References

- 1 W. Miller, Perspective: Quantum or classical coherence?, J. Chem. Phys., 2012, 136, 210901.
- 2 A. J. Leggett, S. Chakravarty, A. T. Dorsey, M. P. A. Fisher, A. Garg and M. Zwerger, Dynamics of the dissipative twostate system, Rev. Mod. Phys., 1987, 59, 1-85.
- 3 H. A. Kramers, Brownian motion an a field of force and the diffusion model of chemical reactions, Physica, 1940, 7, 284-304.
- 4 E. Pollak, Theory of activated rate processes: A new derivation of Kramers' expression, J. Chem. Phys., 1986, 85, 865.
- 5 P. Hänggi, P. Talkner and M. Borcovec, Fifty years after Kramers, Rev. Mod. Phys., 1990, 62, 251-341.
- 6 P. G. Wolynes, Dissipation, tunneling and adiabaticity criteria for curve crossing problems in the condensed phase, J. Chem. Phys., 1987, 86, 1957-1966.
- 7 J. N. Onuchic and P. G. Wolynes, Classical and quantum pictures of reaction dynamics in condensed matter: Resonances, dephasing, and all that, J. Phys. Chem., 1988, 92, 6495-6503.
- 8 F. Webster, P. J. Rossky and R. A. Friesner, Nonadiabatic processes in condensed matter: Semiclassical theory and implementation, Comput. Phys. Commun., 1991, 63, 494-522
- 9 N. Makri, Quantum dissipative systems: a numerically exact methodology, J. Phys. Chem., 1998, 102, 4414-4427.
- 10 W. H. Miller, Quantum and semiclassical theory of chemical reaction rates, Faraday Discuss., 1998, 110, 1-21.
- 11 R. A. Marcus and N. Sutin, Electron transfers in chemistry and biology, Biochim. Biophys. Acta, 1985, 811, 265-322.
- 12 J. Schnitker and P. J. Rossky, Quantum simulation study of the hydrated electron, J. Chem. Phys., 1987, 86, 3471-3485.
- 13 J. I. Kim, M. C. Nemes, A. F. R. de Toledo Piza and H. E. Borges, Perturbative expansion for coherence loss, Phys. Rev. Lett., 1996, 77, 207-210.
- 14 A. K. Pattanayak and P. Brumer, Exponentially rapid decoherence of quantum chaotic systems, Phys. Rev. Lett., 1997, 79, 4131-4134.

- 15 B. Gu and I. Franco, Quantifying early time quantum decoherence dynamics through fluctuations, J. Phys. Chem. Lett., 2017, 8, 4289-4294.
- 16 B. Gu and I. Franco, Generalized theory for the timescale of molecular electronic decoherence in the condensed phase, I. Phys. Chem. Lett., 2018, 9, 773-778.
- 17 B. Gu and I. Franco, Electronic interactions do not affect electronic decoherence in the pure-dephasing limit, J. Chem. Phys., 2018, 149, 174115.
- 18 S. Chatterjee and N. Makri, Recovery of purity in dissipative tunneling dynamics, J. Phys. Chem. Lett., 2020, 11, 8592-8596.
- 19 Y. Elran and P. Brumer, Decoherence in an anharmonic oscillator coupled to a thermal environment: A semiclassical forward-backward approach, J. Chem. Phys., 2004, 121, 2673-2684.
- 20 N. Makri, Exploiting classical decoherence in dissipative quantum dynamics: Memory, phonon emission, and the blip sum, Chem. Phys. Lett., 2014, 593, 93-103.
- 21 J. Gong and P. Brumer, When is quantum decoherence dynamics classical?, Phys. Rev. Lett., 2003, 90, 050402.
- 22 A. O. Caldeira and A. J. Leggett, Path integral approach to quantum Brownian motion, Phys. A, 1983, 121, 587-616.
- 23 A. Bose and N. Makri, Non-equilibrium reactive flux: A unified framework for slow and fast reaction kinetics, J. Chem. Phys., 2017, 147, 152723.
- 24 S. Chatterjee and N. Makri, Density matrix and purity evolution in dissipative two-level systems: II. Relaxation, Phys. Chem. Chem. Phys., 2021, DOI: 10.1039/d0cp05528j.
- 25 R. P. Feynman, Space-time approach to non-relativistic quantum mechanics, Rev. Mod. Phys., 1948, 20, 367-387.
- 26 R. P. Feynman and A. R. Hibbs, Quantum Mechanics and Path Integrals, McGraw-Hill, New York, 1965.
- 27 R. P. Feynman and F. L. Vernon, The theory of a general quantum system interacting with a linear dissipative system, Ann. Phys., 1963, 24, 118-173.
- 28 N. Makri, Dynamics of reduced density matrices: classical memory vs. quantum nonlocality, J. Chem. Phys., 1998, 109, 2994-2998.
- 29 R. Lambert and N. Makri, Quantum-classical path integral: Classical memory and weak quantum nonlocality, J. Chem. Phys., 2012, 137, 22A552.
- 30 N. Makri, Improved Feynman propagators on a grid and non-adiabatic corrections within the path integral framework, Chem. Phys. Lett., 1992, 193, 435-444.
- 31 N. Makri and D. E. Makarov, Tensor multiplication for iterative quantum time evolution of reduced density matrices. I. Theory, J. Chem. Phys., 1995, 102, 4600-4610.
- 32 N. Makri and D. E. Makarov, Tensor multiplication for iterative quantum time evolution of reduced density matrices. II. Numerical methodology, J. Chem. Phys., 1995, 102, 4611-4618.
- 33 N. Makri, Blip decomposition of the path integral: Exponential acceleration of real-time calculations for quantum dissipative systems, J. Chem. Phys., 2014, 141, 134117.
- 34 N. Makri, Iterative blip-summed path integral for quantum dynamics in strongly dissipative environments, J. Chem. Phys., 2017, 146, 134101.

- 35 N. Makri, Small matrix disentanglement of the path integral: overcoming the exponential tensor scaling with memory length, J. Chem. Phys., 2020, 152, 041104.
- 36 N. Makri, Small matrix path integral for system-bath dynamics, J. Chem. Theory Comput., 2020, 16, 4038-4049.
- 37 R. E. Blankenship, Molecular mechanisms of photosynthesis, World Scientific, London, 2002.
- 38 J. Frenkel, On the transforation of light into heat in solids, Phys. Rev., 1931, 37, 17.
- 39 L. Valkunas; H. V. Amerongen and R. Van Grondelle, Photosynthetic excitons, World Scientific, 2000.
- 40 V. May and O. Kühn, Charge and energy transfer dynamics in molecular systems, 3rd edn, Wiley, 2011.
- 41 S. Tretiak, C. Middleton, V. Chernyak and S. Mukamel, Exciton Hamiltonian for the bacteriochlorophyll system in the LH2 antenna complex of purple bacteria, J. Phys. Chem. B, 2000, **104**, 4519-4528.
- 42 A. Ishizaki and G. R. Fleming, Theoretical examination of quantum coherence in a photosynthetic system at physiological temperature, Proc. Natl. Acad. Sci. U. S. A., 2009, 106, 17255-17260.
- 43 V. Tiwari, W. K. Peters and D. M. Jonas, Electronic energy transfer through non-adiabatic vibrational-electronic resonance. I. Theory for a dimer, J. Chem. Phys., 2017, 147, 154308.
- 44 H.-G. Duan, V. I. Prokhorenko, R. J. Cogdell, K. Ashraf, A. L. Stevens, M. Thorwart and R. J. D. Miller, Nature does not rely on long-lived electronic quantum coherence for photosynthetic energy transfer, Proc. Natl. Acad. Sci. U. S. A., 2017, 201702261.
- 45 A. Strathearn, P. Kirton, D. Kilda, J. Keeling and B. W. Lovett, Efficient non-Markovian quantum dynamics using time-evolving matrix product operators, Nat. Commun., 2018, 9, 3322.
- 46 S. Savikhin, D. R. Buck and W. S. Struve, Oscillating anisotropies in a bacteriochlorophyll protein: Evidence for quantum beating between exciton levels, Chem. Phys., 1997, 223, 303-312.
- 47 G. S. Engel, T. R. Calhoun, E. L. Read, T.-K. Ahn, T. Mančal, Y.-C. Cheng, R. E. Blankenship and G. R. Fleming, Evidence for wavelike energy transfer through quantum coherence in photosynthetic systems, Nature, 2007, 446, 782-786.
- 48 T. R. Calhoun, N. S. Ginsberg, G. S. Schlau-Cohen, Y.-C. Cheng, M. Ballottari, R. Bassi and G. R. Fleming, Quantum coherence enabled determination of the energy landscape in light-harvesting complex II, J. Phys. Chem. B, 2009, 113, 16291-16295.
- 49 E. Collini, C. Y. Wong, K. E. Wilk, P. M. G. Curmi, P. Brumer and G. D. Scholes, Coherently wired light-harvesting in photosyntheticmarine algae at ambient temperature, Nature, 2010, 463, 644.
- 50 D. M. Jonas, Two-dimensional femtosecond spectroscopy, Annu. Rev. Phys. Chem., 2003, 54, 425-463.
- 51 T. Brixner, I. V. Stiopkin and G. R. Fleming, Phase-stabilized two-dimensional electronic spectroscopy, J. Chem. Phys., 2004, 121, 4221.

Paper

52 P. Bhattacharyya and G. R. Fleming, Two-dimensional electronic-vibrational spectroscopy of coupled molecular complexes: A near-analytical approach, *J. Phys. Chem. Lett.*, 2019, **10**, 2081–2089.

- 53 A. J. Kiessling and J. A. Cina, Monitoring the evolution of intersite and interexciton coherence in electronic excitation transfer via wave-packet interferometry, *J. Chem. Phys.*, 2020, **152**, 244311.
- 54 M. Rätsep, Z.-L. Cai, J. R. Reimers and A. Freiberg, Demonstration and interpretation of significant asymmetry in the low-resolution and high-resolution Qy fluorescence and absorption spectra of bacteriochlorophyll a, J. Chem. Phys., 2011, 134, 024506.
- 55 T. Renger, V. May and O. Kühn, Ultrafast excitation energy transfer dynamics in photosynthetic pigment-protein complexes, *Phys. Rep.*, 2001, 343, 137–254.
- 56 H.-G. Duan, A. L. Stevens, P. Nalbach, M. Thorwart, V. I. Prokhorenko and R. J. D. Miller, Two-dimensional electronic spectroscopy of light-harvesting complex II at ambient temperature: A joint experimental and theoretical study, J. Phys. Chem. B, 2015, 119, 12017–12027.
- 57 J. Cao, R. J. Cogdell, D. F. Coker, H.-G. Duan, J. Hauer, U. Kleinekathöfer, T. L. C. Jansen, T. Mančal, R. J. D. Miller, J. P. Ogilvie, V. I. Prokhorenko, T. Renger, H.-S. Tan, R. Tempelaar, M. Thorwart, E. Thyrhaug, S. Westenhoff and D. Zigmantas, Quantum biology revisited, *Sci. Adv.*, 2020, 6, eaaz4888.
- 58 A. Bose and N. Makri, Quantum-classical path integral all-mode simulation of exciton-vibration dynamics in the bacteriochlorophyll dimer, *J. Phys. Chem.*, 2020, 124, 5028–5038.

- 59 S. Kundu and N. Makri, Real-time path integral simulation of exciton-vibration dynamics in light-harvesting bacteriochlorophyll aggregates, *J. Phys. Chem. Lett.*, 2020, 11, 8783–8789.
- 60 R. Lambert and N. Makri, Quantum-classical path integral: Numerical formulation, *J. Chem. Phys.*, 2012, 137, 22A553.
- 61 N. Makri, Quantum-classical path integral: A rigorous approach to condensed phase dynamics, *Int. J. Quantum Chem.*, 2015, **115**, 1209–1214.
- 62 P. L. Walters and N. Makri, Iterative quantum-classical path integral with dynamically consistent state hopping, *J. Chem. Phys.*, 2016, **144**, 044108.
- 63 N. Makri, Blip-summed quantum-classical path integral with cumulative quantum memory, *Faraday Discuss.*, 2016, 195 81–92
- 64 F. Wang and N. Makri, Quantum-classical path integral with a harmonic treatment of the back-reaction, *J. Chem. Phys.*, 2019, **150**, 184102.
- 65 N. Makri, Modular path integral: Quantum dynamics via sequential necklace linking, *J. Chem. Phys.*, 2018, **148**, 101101.
- 66 N. Makri, Modular path integral methodology for real-time quantum dynamics, *J. Chem. Phys.*, 2018, **149**, 214108.
- 67 S. Kundu and N. Makri, Modular path integral for discrete systems with non-diagonal couplings, *J. Chem. Phys.*, 2019, **151**, 074110.
- 68 S. Kundu and N. Makri, Efficient matrix factorisation of the modular path integral for extended systems, *Mol. Phys.*, 2020, 1–14, DOI: 10.1080/00268976.2020.1797200.